On the existence and stability of electrostatic structures in non-Maxwellian electron-positron-ion plasmas

Published in:
Physics of Plasmas

Document Version:
Publisher's PDF, also known as Version of record

Queen's University Belfast - Research Portal:
Link to publication record in Queen's University Belfast Research Portal

Publisher rights
2013 AIP Publishing LLC

On the existence and stability of electrostatic structures in non-Maxwellian electron-positron-ion plasmas

G. Williams and I. Kourakis

On the existence and stability of electrostatic structures in non-Maxwellian electron-positron-ion plasmas

G. Williams[a)] and I. Kourakis[b)]

Centre for Plasma Physics, Department of Physics and Astronomy, Queen's University Belfast,
Belfast BT7 1NN, Northern Ireland, United Kingdom

Electrostatic solitary waves in plasmas are the focus of many current studies of localized electrostatic disturbances in both laboratory and astrophysical plasmas. Here, an investigation of the nonlinear dynamics of plasma evolving in two dimensions, in the presence of excess superthermal background electrons and positrons, is undertaken. We investigate the effect of a magnetic field on weakly nonlinear ion acoustic waves. Deviation from the Maxwellian distribution is effectively modelled by the kappa model. A linear dispersion relation is derived, and a decrease in frequency and phase speed in both parallel and perpendicular modes can be seen, when the proportion of positrons to electrons increases. We show that ion acoustic solitary waves can be generated during the nonlinear evolution of a plasma fluid, and their nonlinear propagation is governed by a Zakharov-Kuznetsov (ZK) type equation. A multiple scales perturbation technique is used to derive the ZK equation. The solitary wave structures are dependent on the relation between the system parameters, specifically the superthermality of the system, the proportion of positron content, magnetic field strength, and the difference between electron and positron temperature. The parametric effect of these on electrostatic shock structures is investigated. In particular, we find that stronger superthermality leads to narrower excitations with smaller potential amplitudes. Increased positron concentration also suppresses both the amplitude and the width of solitary wave structures. However, the structures are only weakly affected by temperature differentials between electrons and positrons in our model. © 2013 AIP Publishing LLC. [http://dx.doi.org/10.1063/1.4849415]

I. INTRODUCTION

Electrostatic solitary waves in plasmas are the focus of many current studies of localized electrostatic disturbances in both laboratory and astrophysical plasmas. A great deal of attention has been paid to astrophysical systems and space plasmas that are observed to have so-called superthermal distribution functions, that is, distributions with high energy tails or pronounced shoulders.[1–6] For example, observations and *in situ* measurements have confirmed the wide-spread existence of superthermal populations at different altitudes in the solar wind plasma,[3,4,7] in Earth's magnetospheric plasma sheet,[5,8] and in Saturn.[2,9]

Such distribution functions may be well fitted by the so-called kappa distribution, as was shown for the first time by Vasyliunas,[1] as well as by Maksimovic *et al.*,[7] Formisano *et al.*,[8] Schippers *et al.*,[9] and Hellberg *et al.*[10] The spectral index, kappa (κ), for which the kappa distribution is named, acts to modify the effective thermal speed in the distribution function. At low values of κ, distributions have a large component of superthermal particles, but at very large values of kappa, the distribution function approaches a Maxwellian distribution. At present, although the kappa distribution is quite successful in modelling superthermal plasmas, there is as yet no rigorous theoretical foundation for kappa distribution theory.

It should be noted that there is more than one version of the kappa distribution expression in literature. Considering the comment by Hellberg *et al.*,[10] we utilize below the original version of the distribution,[1] as employed by Sultana *et al.*,[11,12] Baluku and Hellberg[13] and many others, rather than that used in papers by Hau and Fu[14] and El-Bedwehy and Moslem.[15]

Electron-positron-ion (e-p-i) plasmas may be either partially or fully ionized gases depending upon the plasma parameters, and are found not only in the early universe[16,17] but also in astrophysical environments such as in the magnetosphere of pulsars,[18] active galactic nuclei (AGN),[19] in neutron star atmospheres,[20] in the inner regions of accretion disks surrounding black holes,[21,22] and the interstellar medium.[23,24]

In the laboratory, the production of electron-positron pairs by the interaction of relativistic superthermal electrons with high Z material was shown by Liang *et al.*,[25] and the existence of positrons in plasmas has also been confirmed in other laboratory plasmas.[26–28] The process of electron-positron pair production can also occur during the interaction of a strong laser pulse with plasmas.[29,30] This creation of large numbers of MeV positrons in the laboratory has led to more antimatter research, including investigation of the physics underlying various astrophysical phenomena such as black holes and gamma ray bursts, positronium production and Bose-Einstein condensates. Chen *et al.*[31] illuminated gold targets with short ultraintense laser pulses, and positrons of up to 2×10^{10} per steradian were observed to emerge from the back of the target, with effective temperatures of almost 3 MeV, which was found to be approximately half

---
a)E-mail: gwilliams06@qub.ac.uk
b)www.kourakis.eu

that of the effective electron temperature. Electron-positron and γ-photon production by a high-intensity laser pulse was also investigated[32] using two 330 femtosecond laser pulses and the positron density was found to be 5×10^{22} cm^{-3}. Pair production was also studied for underdense plasmas and plasma channels.[33] In this context, the number of relativistic electrons can be high, because the laser pulse can propagate a long distance, whereas the density is limited by the critical density for the laser pulse. Various mechanisms can be found for the production of electron-positron pairs by intense focused laser light pulses. (See, for example, Refs. 34 and 35, and the references therein.) Thus, the study of the properties of e-p-i plasmas in the presence of strong and super-strong laser pulses or non-thermal equilibrium cosmic field radiation is of much interest. In particular, we are inspired by recent experimental results on positron production in the laboratory,[36,37] as well as currently unpublished results on pair-plasma production via table-top laser based procedures[38] which will clearly generate even more interest on this topic.

Interestingly, the presence of ions enables the existence of low frequency waves such as ion-acoustic waves, which otherwise could not propagate in electron-positron (e-p) plasmas. Nonlinear techniques can be used to investigate electrostatic excitations that may arise in e-p-i plasmas. The Zakharov-Kuznetsov (ZK) equation,[39] derived in 1974 (Ref. 40) for ion-acoustic waves in a magnetized plasma, is a multi-dimensional extension of the well-known Korteweg-de Vries (KdV) equation. In recent years, several studies have utilized ZK type equations to investigate the nonlinear characteristics of e-p-i plasmas.[41–43] Kourakis et al.[41] investigated the existence and properties of nonlinear electrostatic structures in rotating magnetized e-p-i plasmas using the ZK equation, and showed that the balance among dispersion and nonlinearity gives rise to localized solitary wave solutions. Qu et al.[42] looked at soliton solutions of the ZK equation in e-p-i plasmas and their interactions, and utilising the Hirota method, found an N-soliton solution. El-Shamy and El-Bedwehy[43] also investigated nonlinear electrostatic solitary waves in e-p-i magnetoplasmas using both the ZK equation, and studied their compressive and rarefactive nature.

In this paper, we study ion acoustic waves in a magnetized plasma with excess kappa distributed superthermal electrons and kappa distributed positrons, building on previous research.[41,42,44] We investigate the solitary solutions of the ZK equation and address two separate situations—the first is the e-p-i plasmas likely to arise in laboratory plasmas which are close to the e-i limit (so very few positrons present). The second situation is at the other extreme, typical in astrophysical plasmas, where the plasma is close to the e-p limit (so very few ions present). The paper is organized in the following manner. In Sec. II, we present the relevant fluid equations for ion acoustic waves in a magnetized e-p-i plasma. Section III details the linear behaviour of the system. We derive the dispersion relation and discuss the effects of variation in positron content and temperature variation between electrons and positrons. In Sec. IV, a reductive perturbation technique is used[45] to derive the ZK equation.[46] Solitary wave solutions to the ZK equation are found in

Sec. V, and the stability of these solutions is considered in Sec. VI. In Sec. VII, a parametric investigation is undertaken, in terms of relevant plasma parameters, looking separately at low positron content plasmas (Regime A) and high positron content plasmas (Regime B). Some alternative solutions are discussed in Sec. VIII, and finally, our results are summarized in Sec. IX.

II. THE FLUID EQUATION MODEL

We are modelling ion-acoustic waves propagating in a magnetized electron-positron-ion plasma. The magnetic field $\mathbf{B_0}$ is uniform and for simplicity we choose for it to lie along the z-axis of our Cartesian coordinate system. The plasma consists of cold ions, kappa-distributed electrons, and kappa-distributed positrons. At equilibrium, we assume that $Z_i n_{i0} + n_{p0} = n_{e0}$, where n_{i0}, n_{p0}, and n_{e0} are the equilibrium ion, positron and electron number densities, respectively; and Z_i is the charge state of the ions. We employ the following system of equations:

$$\frac{\partial n_i}{\partial t} + \nabla n_i \mathbf{u_i} = 0, \qquad (1)$$

$$\frac{\partial \mathbf{u_i}}{\partial t} + \mathbf{u_i} \nabla \mathbf{u_i} = \left(\frac{Z_i e}{m}\right)(-\nabla \phi + \mathbf{u_i} \times B_0 \hat{z}), \qquad (2)$$

with the system closed by Poisson's equation

$$\epsilon_0 \nabla^2 \phi = e(n_e - Z_i n_i - n_p), \qquad (3)$$

where n_i, n_e, n_p, and $\mathbf{u_i}$ are ion density, electron density, positron density and ion velocity, respectively; ϕ is the electric potential; and e and m_i are the unit charge and ion mass, respectively. The electron and positron densities are characterized by kappa distributions[1]

$$n_e = n_{e0}\left(1 - \frac{e\phi}{(\kappa_e - 3/2)k_B T_e}\right)^{-\kappa_e + 1/2} = n_{e0} f_e(\phi),$$

and

$$n_p = n_{p0}\left(1 + \frac{e\phi}{(\kappa_p - 3/2)k_B T_p}\right)^{-\kappa_p + 1/2} = n_{p0} f_p(\phi),$$

where the real parameters κ_e (for electrons) and κ_p (for positrons) measure the deviation from Maxwellian equilibrium, which is recovered in the limit of infinite κ at every step.[1,47] Note that k_B is Boltzmann's constant, and T_e and T_p are the electron and positron temperatures, respectively. Note that ionic thermal effects have been neglected in this model.

To make the calculations tractable analytically, we have employed the following normalizations: we have normalized lengths by a characteristic Debye length $\lambda_D = (\frac{\epsilon_0 k_B T_e}{n_{i0} Z_i^2 e^2})^{\frac{1}{2}}$, time by the inverse ion plasma frequency $\omega_{pi} = (\frac{n_{i0} Z_i^2 e^2}{\epsilon_0 m_i})^{\frac{1}{2}}$, number density by the total ion density n_{i0}, electrostatic potential by $(\frac{k_B T_e}{Z_i e})$, velocities by the ion-acoustic sound speed $c_{i,s} = (\frac{k_B T_e}{m_i})^{\frac{1}{2}}$ and the magnetic field is represented by $\Omega = \omega_{ci}/\omega_{pi}$, which

is the ratio of the ion cyclotron frequency ($\omega_{ci} = \frac{Z_i e B_0}{m_i}$) to the ion plasma frequency ($\omega_{pi} = (\frac{Z_i^2 n_0 e^2}{\epsilon_0 m_i})^{1/2}$).

We also utilize the following definitions: $\theta = \frac{T_p}{T_e}$, $\delta = \frac{n_{p0}}{n_{e0}}$, which represent the ratio of positron temperature to electron temperature, and the ratio of positron density to electron density, respectively. It follows that $\frac{n_{e0}}{Z_i n_{i0}} = \frac{1}{1-\delta}$, and $\frac{n_{p0}}{Z_i n_{i0}} = \frac{\delta}{1-\delta}$. At δ near 0, we have a quasi electron-ion (e-i) plasma, with very few positrons present, typical of a laboratory plasma. At δ near 1, we have a quasi electron-positron (e-p) plasma with a small population of minority ions, typical of astrophysical plasmas, and where we expect the role of θ to be more pronounced.

We have expanded Eq. (3) using a Taylor series, truncated at second order, and so achieve the following dimensionless system of equations:

$$\frac{\partial n}{\partial t} + \nabla n\mathbf{u} = 0, \qquad (4)$$

$$\frac{\partial \mathbf{u}}{\partial t} + \mathbf{u}\nabla\mathbf{u} = -\nabla\phi + \mathbf{u} \times \Omega\hat{\mathbf{z}}, \qquad (5)$$

$$\nabla^2\phi \approx 1 + p\phi + q\phi^2 - n, \qquad (6)$$

where

$$p = \frac{1}{Z_i(1-\delta)}\left[\left(\frac{2\kappa_e - 1}{2\kappa_e - 3}\right) + \frac{\delta}{\theta}\left(\frac{2\kappa_p - 1}{2\kappa_p - 3}\right)\right],$$

$$q = \frac{1}{2Z_i^2(1-\delta)}\left[\left(\frac{4\kappa_e^2 - 1}{(2\kappa_e - 3)^2}\right) - \frac{\delta}{\theta^2}\left(\frac{4\kappa_p^2 - 1}{(2\kappa_p - 3)^2}\right)\right]. \qquad (7)$$

We note that $p = 2q = 1$ is recovered in the Maxwellian e-i limit (with Z_i set to 1 and $\delta = 0$).

III. LINEAR ANALYSIS

We linearize the system of fluid equations and form a homogeneous system of 3 algebraic equations in the three variables n_i, u, ϕ, which can be solved to give the linear dispersion equation

$$\omega^4 - \omega^2\left(\Omega^2 + \omega_0^2\right) + \omega_0^2\Omega^2 - \frac{k_\perp^2}{k^2 + p}\Omega^2 = 0, \qquad (8)$$

where p is given by Eq. (7) above, $k_\parallel$ and $k_\perp$ are wavenumber components parallel and perpendicular to the magnetic field, respectively, so that $k^2 = k_\parallel^2 + k_\perp^2$; and $\omega_0^2 = k^2/(k^2 + p)$ is the linear dispersion relation of ion-acoustic waves in a non-magnetized plasma.

We can also usefully express the dispersion relation in terms of ω^2 as

$$\omega_\pm^2 = \frac{1}{2}\left[\omega_0^2 + \Omega^2 \pm \sqrt{(\omega_0^2 - \Omega^2)^2 + \frac{4k_\perp^2\Omega^2}{k^2 + p}}\right]. \qquad (9)$$

This equation leads to two separate modes of propagation, as shown in Figure 1, which displays the dispersion relation for three different values of δ. The upper plot shows both the
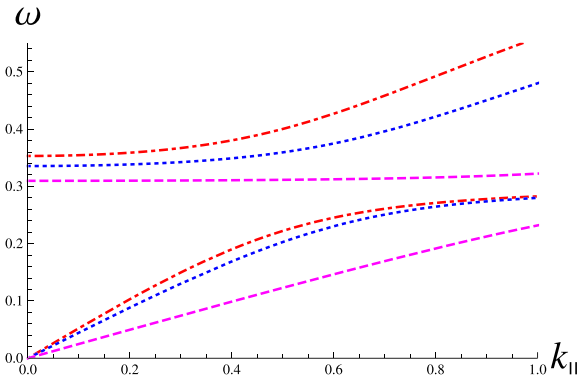

FIG. 1. Linear dispersion relation based on Eq. (9). The upper plot shows both modes, and the lower plot zooms in on the acoustic mode only. In both plots, the dotted-dashed (red) line is for $\delta = 0.2$, the dotted (blue) line is $\delta = 0.4$, and the dashed (purple) line is $\delta = 0.8$. Here, we have taken $\Omega = 0.09$, $\kappa = 3$, $\theta = 1$ and set the perpendicular component of k, $k_\perp = 0.3$.

upper and lower modes, which decrease in frequency with increasing δ, but the lower mode decrease is very small and only noticeable for small values of k (long wavelength values). The lower plot in Figure 1 zooms in on this lower mode, and importantly we note that it is an acoustic mode, that is, it satisfies $\lim_{k\to 0}(\omega_-) = 0$. We will consider quasi-parallel propagation below (in the next Section), hence the phase speed of relevance will be: $\lim_{k_\parallel\to 0}(\omega_-/k_\parallel) = \frac{1}{\sqrt{p}}$. This is essentially the phase speed of the lower (acoustic) mode in the long wavelength ($k \ll 1$) region. In other words, it is precisely the true sound speed in the given plasma configuration. Figure 2 shows the same dispersion relation, but this time with varying temperature differential between electrons and positrons (changing θ in the equation). We find that varying θ has very little effect on the linear dispersion, in either the upper or lower mode.

Limiting Case 1—no magnetic field: If the magnetic field is so weak that we can neglect it, Eq. (9) reduces to: $\omega^2 = \omega_0^2(k)$, which describes an ion acoustic wave in a non-magnetized plasma.

Limiting Case 2—parallel propagation: If we consider only waves propagating parallel to the magnetic field ($k_\perp \to 0$), Eq. (9) becomes
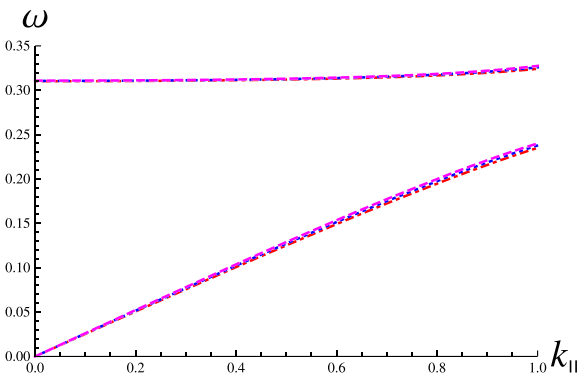

FIG. 2. Linear dispersion relation based on Eq. (9). The dotted-dashed (red) line is for $\theta = 1.1$, the dotted (blue) line is $\theta = 1.2$, and the dashed (purple) line is $\theta = 1.3$. Here, we have taken $\kappa = 3$, $\delta = 0.2$, $\Omega = 0.09$ and set the perpendicular component of k, $k_\perp = 0.3$.

$$\omega^2 = \frac{1}{2}\left[\frac{k_\parallel^2}{k_\parallel^2+p}+\Omega^2 \pm \left(\frac{k_\parallel^2}{k_\parallel^2+p}-\Omega^2\right)\right]. \qquad (10)$$

This leads to two solutions: the trivial solution $\omega^2 = \Omega^2$, which we can neglect as it is non-propagating, and $\omega^2 = \frac{k_\parallel^2}{k_\parallel^2+p}$, which (upon setting $k = k_\parallel$) is equivalent to ω_0^2 above, the ion-acoustic wave linear dispersion relation seen in the unmagnetized case. This is expected, as in parallel propagation the vector cross product of the velocity with the magnetic field is equal to zero, and so the wave dispersion is unaffected by the magnetic field.

Limiting Case 3—perpendicular propagation: If we consider only waves propagating perpendicularly to the magnetic field ($k_\parallel \to 0$), Eq. (9) leads to: $\omega^2 = \frac{k_\perp^2}{k_\perp^2+p}+\Omega^2$, which is a dispersion relation describing low frequency magnetoacoustic waves, as described by Swanson.[48]

Overall, there is a decrease in frequency and phase speed in both parallel and perpendicular modes due to excess superthermal positrons, discernible in both the upper mode and the lower (acoustic) mode.

IV. REDUCTIVE PERTURBATION THEORY

To investigate the nonlinear behaviour of the small ion acoustic waves, we use reductive perturbation theory, in which the independent variables are stretched as follows: $X = \varepsilon^{\frac{1}{2}}x$; $Y = \varepsilon^{\frac{1}{2}}y$; $Z = \varepsilon^{\frac{1}{2}}(z - \mathbb{V}t)$; $T = \varepsilon^{\frac{3}{2}}t$, where $\mathbb{V}$ is a speed to be determined.

We have assumed that the ion streaming velocity is along the z-axis, and expand in the wave amplitude while keeping one order higher than in linear theory. Due to the anisotropy introduced into the system by the magnetic field, the coordinates of velocity perpendicular to the magnetic field, u_x and u_y appear at higher order in ε than the parallel component u_z. This means that the gyromotion is treated as a higher order effect in this model

$$\bar{n}_i = 1 + \varepsilon n_1 + \varepsilon^2 n_2 + \ldots, \quad \bar{\phi} = \varepsilon\phi_1 + \varepsilon^2\phi_2 + \ldots,$$
$$\bar{u}_x = \varepsilon^{\frac{3}{2}}u_{x1} + \varepsilon^2 u_{x2} + \ldots, \quad \bar{u}_y = \varepsilon^{\frac{3}{2}}u_{y1} + \varepsilon^2 u_{y2} + \ldots,$$
$$\bar{u}_z = \varepsilon u_{z1} + \varepsilon^2 u_{z2} + \ldots.$$

We substitute the stretched variables above into our dimensionless set of fluid equations, and extract the lowest order terms to produce a series of compatibility conditions, which allows us to express n_1, u_{x1}, u_{y1}, and u_{z1} in terms of ϕ_1 as follows:

$$n_1 = p\phi_1,$$
$$\frac{\partial u_{z1}}{\partial Z} = \mathbb{V}\frac{\partial n_1}{\partial Z} = \frac{1}{\mathbb{V}}\frac{\partial\phi_1}{\partial Z},$$
$$\Omega u_{y1} = \frac{\partial\phi_1}{\partial X}, \qquad (11)$$
$$\Omega u_{x1} = \frac{\partial\phi_1}{\partial Y}.$$

Combining these expressions allows us to express the speed $\mathbb{V}$ as

$$\mathbb{V} = p^{-1/2}, \qquad (12)$$

where p is given by Eq. (7). $\mathbb{V}$ is thus dependent on the electron and positron κ parameters, the ratio of positron to electron density, δ, and the ratio of positron to electron temperature, θ. We notice that the method provides Eq. (12) as a compatibility condition, which prescribes the stationary pulse speed $\mathbb{V}$ as the true sound speed. Figure 3 shows how the phase velocity changes with increase in positron content and superthermality. Lower values of kappa indicate strong superthermality, and we see that the phase speed is significantly reduced at low values of kappa. As $\kappa \to \infty$, $\mathbb{V} \to 1$, which represents the normalized sound speed in Maxwellian conditions. These comments agree with earlier considerations in literature, for example, Eq. (21) in Ref. 47 (in which M_1 is equivalent to our $\mathbb{V}$), and also Sec. III in Ref. 12. Additionally, the phase speed also reduces with increasing positrons, approaching zero as $\delta \to 1$.

The second order terms yield a further set of compatibility conditions, which when combined with the 1st order conditions above, lead to the derivation of a ZK type equation

$$\frac{\partial\phi_1}{\partial T} + A\phi_1\frac{\partial\phi_1}{\partial Z} + B\frac{\partial^3\phi_1}{\partial Z^3} + C\frac{\partial}{\partial Z}\left(\frac{\partial^2\phi_1}{\partial X^2}+\frac{\partial^2\phi_1}{\partial Y^2}\right) = 0,$$
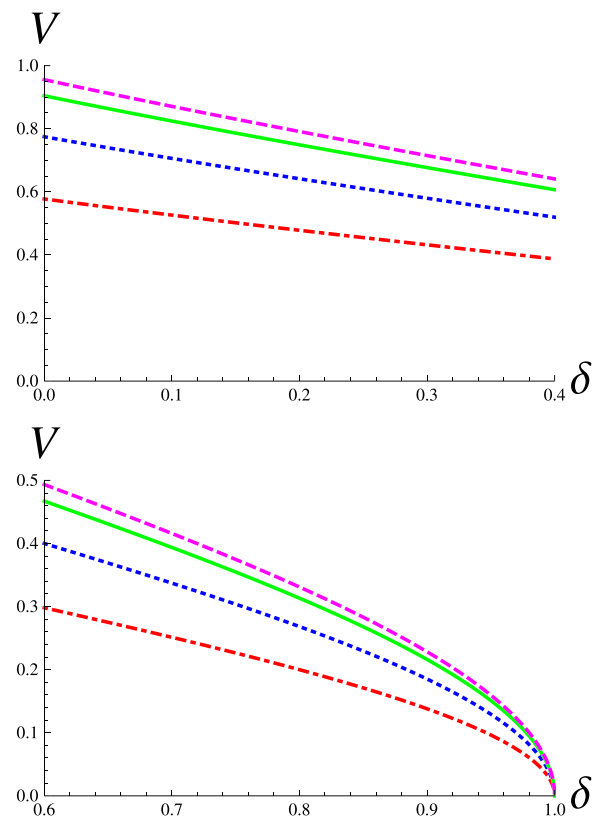
$$(13)$$

FIG. 3. The variation of phase velocity $\mathbb{V}$ with δ. Upper plot: Regime A, plasma with a small percentage of positrons, and lower plot, Regime B, plasma with large percentage of positrons. In both plots, the dotted-dashed (red) line is for $\kappa = 2$, the dotted (blue) line is $\kappa = 3$, the continuous (green) line is $\kappa = 6$, and the dashed (purple) line is $\kappa = 12$. Here, we have taken $\theta = 1.2$.

where the nonlinearity coefficient A, and dispersion coefficients B and C are defined as

$$A = \frac{3}{2}\frac{1}{Z_i(1-\delta)}\left[\left(\frac{2\kappa_e-1}{2\kappa_e-3}\right)+\frac{\delta}{\theta}\left(\frac{2\kappa_p-1}{2\kappa_p-3}\right)\right]^{1/2}$$
$$-\frac{1}{2Z_i}\frac{\left[\left(\frac{4\kappa_e^2-1}{(2\kappa_e-3)^2}\right)-\frac{\delta}{\theta^2}\left(\frac{4\kappa_p^2-1}{(2\kappa_p-3)^2}\right)\right]}{\left[\left(\frac{2\kappa_e-1}{2\kappa_e-3}\right)+\frac{\delta}{\theta}\left(\frac{2\kappa_p-1}{2\kappa_p-3}\right)\right]^{3/2}}, \qquad (14)$$

$$B = \frac{1}{2}\frac{1}{Z_i(1-\delta)}\left[\left(\frac{2\kappa_e-1}{2\kappa_e-3}\right)+\frac{\delta}{\theta}\left(\frac{2\kappa_p-1}{2\kappa_p-3}\right)\right]^{-3/2},$$

$$C = B\left(1+\frac{1}{\Omega^2}\right).$$

If we look at the Maxwellian electron-ion limit, whereby κ_e and $\kappa_p \to \infty$, $\delta = 0$, and also take $Z_i \to 1$, Eq. (14) reduces to: $A = 1, B = \frac{1}{2}, C = \frac{1}{2}\left(1+\frac{1}{\Omega^2}\right)$. This is the expected result for ion acoustic waves in a magnetized electron-ion plasma, agreeing with Ref. 49 (Eq. (1.2)), Ref. 50 (Eq. (8) therein), and also in agreement with Ref. 12 for coefficients A and B.

V. SOLITARY WAVE SOLUTIONS

This section follows closely the discussion in Ref. 44, thus we proceed by omitting unnecessary details, simply following a layout of relevant results to proceed.

The general solution of Eq. (13) can be found using the hyperbolic tangent (tanh) method,[51] whereby we transform coordinates so that $\phi_1(X,Y,Z,T)=\psi(\chi)$, where $\chi = \alpha(lX+mY+nZ-UT)$, $l^2+m^2+n^2=1$, and U is the incremental soliton velocity (above the sound speed).

Details of the method can be found in Appendix A of Ref. 44 and will be omitted here. We find

$$\psi_{sol} = \psi_0\,\text{sech}^2(\chi), \qquad (15)$$

where $\psi_0 = \frac{3U}{A_0}$ is the amplitude of the excitation, $\chi = \alpha(lX+mY+nZ-UT)$, $\alpha^{-1} = 2\sqrt{\frac{B_0}{U}}$ is the soliton width, $A_0 = An$, $B_0 = Bn^3+Cn(l^2+m^2)$, and A, B, C are as defined previously.

This result agrees with Eq. (24) of Ref. 52, and is a localized solitary wave solution, describing a pulse excitation, in which dispersion and nonlinearity are balanced. Further discussion of their characteristics is discussed below. Interestingly, we may now, based on Eq. (15), derive an exact expression for the electric field vector $\mathbf{E}\,(=-\nabla\psi_{sol})$

$$\mathbf{E} = \begin{pmatrix} E_x \\ E_y \\ E_z \end{pmatrix} = \frac{3U^{3/2}}{A_0 B_0^{1/2}}\,\text{sech}^2\chi\tanh\chi\begin{pmatrix} l\hat{x} \\ m\hat{y} \\ n\hat{z} \end{pmatrix}, \qquad (16)$$

where $\hat{x},\hat{y},\hat{z}$ are the unit vectors in the direction x, y, and z. Note that the magnitude of the electric field is

$$E = \frac{3U^{3/2}}{A_0 B_0^{1/2}}\,\text{sech}^2\chi\tanh\chi, \qquad (17)$$

in agreement with Eq. (28) from Ref. 53, if we substitute U for V therein, and note that L_0 in that equation is the soliton width, equivalent to $\alpha^{-1} = 2\sqrt{\frac{B_0}{U}}$.

VI. STABILITY OF SOLITON SOLUTION

To investigate the stability of the soliton solution above, we shall follow the methodology introduced in Refs. 54 and 55. Using appropriate scaling, as detailed in Appendix A, and transforming $Z \to X$ formally, the ZK equation (13) can be re-written as

$$\partial_t\bar{\phi} + \bar{\phi}\partial_X\bar{\phi} + \partial_X(\partial_X^2+\partial_Y^2+\partial_Z^2)\bar{\phi} = 0, \qquad (18)$$

which is equivalent to Eq. (1.1) in Ref. 55, if we formally set $\bar{\phi} = n$ therein. So by transforming to the geometry used there, we need not repeat Allen and Rowland's stability investigation,[55] but restrict ourselves to summarizing the main points.

Following Allen and Rowlands,[55] we employ the following perturbation:

$$\bar{\phi} = \psi + \epsilon\Phi(x)e^{iky}e^{\gamma t}, \qquad (19)$$

where ψ is precisely the exact solution of Eq. (18). The perturbation is transverse, as the axes in the ZK equation have been rotated so the soliton moves along the x axis. According to this perturbation, if $\text{Re}\gamma = 0$, then the configuration is stable; however for $\text{Re}\gamma \neq 0$, there is instability. One proceeds by substituting the perturbed solution into the ZK equation and linearising in ϵ, which leads to an eigenvalue problem (see Eq. (23) in Ref. 55). In the following, we simply summarize the tedious procedure employed therein. Based on the eigenvalue equation obtained, Allen and Rowlands[55] introduce multiple scales: $x_1 = kx, x_2 = k^2 x$, etc., assuming $k \ll 1$ (physically representing long-wavelength background disturbances, e.g., noise). Accordingly, we also set $\Phi(x) = \Phi_0 + k\Phi_1 + \dots$ and proceed by considering different orders in k. The growth rate for the instability can be expressed as $\Gamma = k\gamma_1 + k^2\gamma_2 + \dots$] neglecting higher order terms. The tedious procedure, omitted here, consists of eliminating secular terms, to find[55]

$$\gamma_1 = \frac{8}{3}\left[\left(\frac{8}{5}\cos^2\beta - 1\right)^{1/2} + i\sin\beta\right]. \qquad (20)$$

So for stability, we require $\frac{8}{5}\cos^2\beta - 1 < 0$, or $\beta > \beta_{cr} = \arccos(\frac{5}{8})^{1/2} \simeq 37.8°$, which recovers exactly[55] the result of Das and Verheest in Ref. 56.

At this stage, stability is ensured for $\beta > \beta_{cr}$. Allen and Rowlands proceed by considering *higher* order (in)stability (related to the real part of γ_2). In an analogous manner, they obtain in their Eq. (2.17)

$$\gamma_2 = -\frac{4}{9}\left(\frac{8}{5}\cos^2\beta - 1\right)\sec\beta + \frac{4(5+4\cos^2\beta)i\tan\beta}{45\left(\frac{8}{5}\cos^2\beta - 1\right)^{1/2}}.$$

$$(21)$$
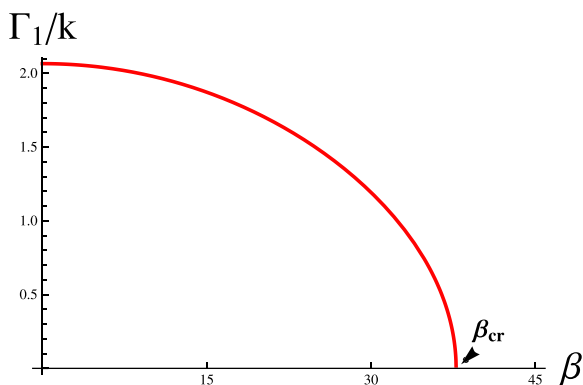
FIG. 4. First order instability growth rate for Γ_1/k. Based on Eq. (22).

In summary, the growth rate of the instability, Γ can be expressed as follows:

If $\beta < \beta_{cr} \simeq 37.8°$, then

$$\Gamma = \Gamma_1 = k\mathrm{Re}(\gamma_1) + \mathcal{O}(k^2)$$
$$\simeq k\frac{8}{3}\left(\frac{8}{5}\cos^2\beta - 1\right)^{1/2}, \qquad (22)$$

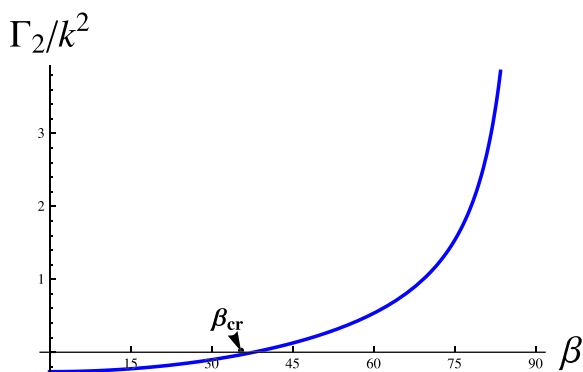If $\beta > \beta_{cr} \simeq 37.8°$, then

$$\Gamma = \Gamma_2 = k^2\mathrm{Re}(\gamma_2) + \mathcal{O}(k^3)$$
$$\simeq k^2\frac{4}{9}\left(1 - \frac{8}{5}\cos^2\beta\right)\sec\beta. \qquad (23)$$

Recall that the above results are valid for $k \ll 1$. Importantly, Allen and Rowlands[55] have also obtained a solution for $k > \cos\beta$, via a numerical analysis. We neglect that result here.

Figure 4 shows the 1st order instability growth rate, and we can see that this reduces to zero as $\beta \to \beta_{cr}$. Figure 5 shows the second order instability growth, which increases for larger values of β.

Now, reverting back to our notation (for details see Appendix B), we find that the growth rate of the instability, Γ, can be expressed in our specific model as follows: If $\beta < \beta_{cr} \simeq 37.8°$, then

FIG. 5. Second order instability growth rate for Γ_2/k^2. Based on Eq. (23).

$$\Gamma = \Gamma_1 = k\mathrm{Re}(\gamma_1) + \mathcal{O}(k^2)$$
$$\simeq k\frac{\sqrt{BC}}{L_\parallel^2}\frac{8}{3}\left(\frac{8}{5}\cos^2\beta - 1\right)^{1/2}. \qquad (24)$$

If $\beta > \beta_{cr} \simeq 37.8°$, then

$$\Gamma = \Gamma_2 = k^2\mathrm{Re}(\gamma_2) + \mathcal{O}(k^3)$$
$$\simeq k^2\frac{C}{L_\parallel}\frac{4}{9}\left(1 - \frac{8}{5}\cos^2\beta\right)\sec\beta. \qquad (25)$$

Here, as noted earlier, C and B are as defined in Eq. (14). We note the explicit dependence of the growth rate on the plasma parameters κ, Ω, and δ via B and C in Eqs. (24) and (25) (see Figures 10 and 15).

VII. PARAMETRIC INVESTIGATION

A. Regime A—low positron content (near the e-i limit). Approximate analysis ($\delta \ll 1$)

The nonlinearity coefficient is represented in our ZK equation by A, while the coefficients B and C represent dispersive terms. A and B are dependent on κ, δ and θ, while C depends additionally on magnetic field strength Ω. Figure 6 shows how A, B, and C are affected by changes in δ.

Close to the e-i limit where $\delta \sim 0$, we can Taylor expand the expressions for A, B, and C to first order and get the following:

$$A \simeq \frac{2(\kappa-1)}{2\kappa-3}\left(\frac{2\kappa-3}{2\kappa-1}\right)^{1/2}$$
$$+ \frac{(1+2\kappa+6\kappa\theta-\theta^2+4\kappa\theta^2)}{2(2\kappa-3)\theta^2}\left(\frac{2\kappa-3}{2\kappa-1}\right)^{1/2}\delta, \qquad (26)$$
$$B \simeq \frac{1}{2}\left(\frac{2\kappa-3}{2\kappa-1}\right)^{3/2} - \frac{3}{4}\left(\frac{2\kappa-3}{2\kappa-1}\right)^{3/2}\frac{1+\theta}{\theta}\delta,$$
$$C = B(1 + 1/\Omega^2).$$

It is clear that the nonlinear and dispersive terms are strongly influenced by the proportion of positrons present in the plasma. At low values of δ, the dispersive coefficient C dominates, but as δ exceeds 0.1, the nonlinear coefficient A
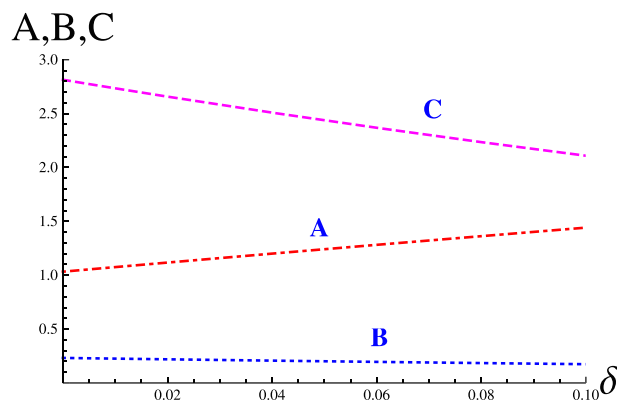
FIG. 6. A, B, C vs δ for values of δ from 0 to 0.4, setting $\Omega = 0.3$, $\kappa_e = \kappa_p = 3$, and $\theta = 1.1$. Based on Eq. (14).
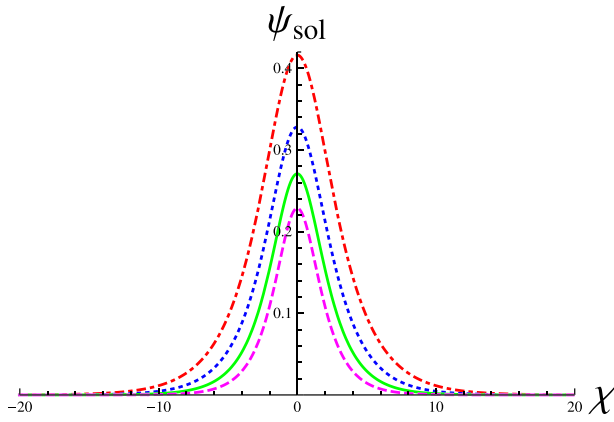
FIG. 7. ψ vs χ for $\delta = 0.1$ (red dotted-dashed line), 0.2 (blue dotted line), 0.3 (green continuous line), and 0.4 (purple dashed line), for the particular orientation where $n = 0.5$, and $l = m = \sqrt{\frac{1-l^2}{2}}$, taking $\Omega = 0.3$, $U = 0.1$, $\kappa_e = \kappa_p = 3$, and $\theta = 1.1$. Based on Eq. (15).

increases steadily and overtakes C which along with B diminishes with increasing positron content, although the effect is not as noticeable for B with the particular values we have taken for Ω and κ.

We can look at the dependence of the solitary wave excitation with a variation in positron content, by changing δ. We see in Figure 7 that the soliton becomes narrower with a reduced potential if the plasma positron content increases.

We now look at how soliton characteristics change with variation in the κ, which represents the degree of superthermality of the plasma. It is worth noting again here that a low value of κ indicates strong superthermality.

Figure 8 suggests that solitons with a low κ value are narrower with smaller amplitude. As κ increases the soliton shape converges to the Maxwellian case. So increasing superthermality leads to lower amplitude and narrower solitons.

We now investigate the effect of a disparity in temperature between electrons and positrons on the solitary excitation in low positron plasmas. We see in Figure 9 that there is only a weak dependence on θ. This is to be expected as it is
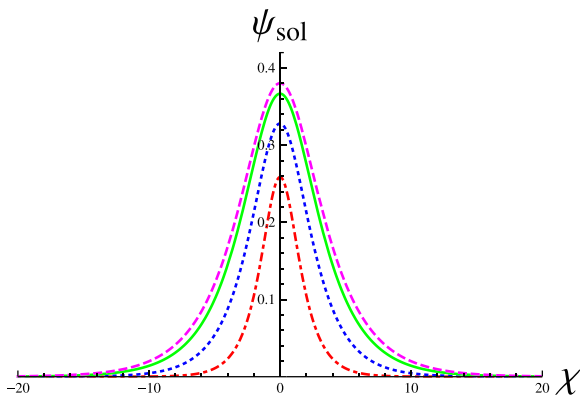

FIG. 8. ψ vs χ for $\kappa = 2$ (red dotted-dashed line), 3 (blue dotted line), 6 (green continuous line), and 12 (purple dashed line), for the particular orientation where $n = 0.5$, and $l = m = \sqrt{\frac{1-l^2}{2}}$, taking $\Omega = 0.3$, $U = 0.1$, $\delta = 0.2$, and $\theta = 1.1$. Based on Eq. (15).
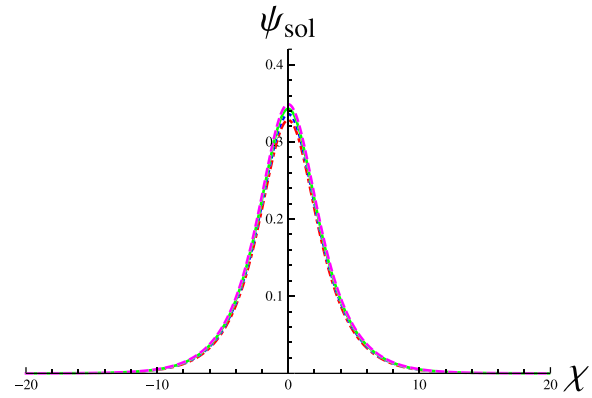

FIG. 9. ψ vs χ for $\theta = 1.1$ (red dotted-dashed line), 1.2 (blue dotted line), 1.3 (green continuous line), and 1.4 (purple dashed line), for the particular orientation where $n = 0.5$, and $l = m = \sqrt{\frac{1-l^2}{2}}$, taking $\Omega = 0.3$, $U = 0.1$, $\delta = 0.2$, and $\kappa = 3$. Based on Eq. (15).

a low positron content plasma, so the temperature difference between positrons and electrons will only affect a small proportion of the plasma constituents.

Finally, we analyse the effect of a change of positron concentration and superthermality on the instability of the soliton solution. In Figure 10, we see in the upper plot that an increase in positron concentration causes the instability growth to be suppressed. In the lower plot, an increase in superthermality also causes a decrease in the growth rate of the instability.
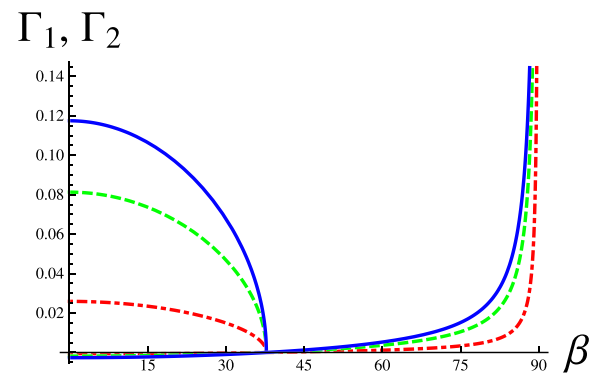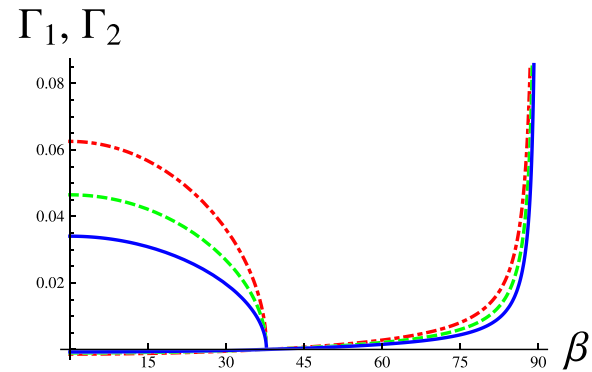

FIG. 10. The first and second order instability growth rate Γ_1 and Γ_2 vs the azimuthal angle β. Upper plot shows $\delta = 0.1$ (red dotted-dashed line), 0.2 (green dashed line), and 0.3 (blue continuous line), taking $\Omega = 0.3$, $\theta = 1.1$, $\kappa = 3$, and wavenumber $k = 0.05$. Lower plot shows $\kappa = 2$ (red dotted-dashed line), 4 (green dashed line), and 12 (blue continuous line), taking $\Omega = 0.3$, $\theta = 1.1$, $\delta = 0.1$, and wavenumber $k = 0.05$. Based on Eqs. (24) and (25).

B. Regime B—high positron content (quasi e-p plasmas). Approximate analysis ($\delta \lesssim 1$)

We now look at plasmas that have a high proportion of positrons. These plasmas are likely to be found in astrophysical scenarios.

Close to the electron-positron limit where $\delta \sim 1$, we can Taylor expand the expressions for A, B, and C to first order and get the following:

$$A \simeq \frac{3}{2}\left(\frac{(2\kappa-1)(1+\theta)}{(2\kappa-3)\theta}\right)^{1/2}\frac{1}{\sqrt{\delta-1}},$$
$$B \simeq \frac{1}{2}\left(\frac{(2\kappa-3)\theta}{(2\kappa-1)(1+\theta)}\right)^{3/2}(1-\delta)^{3/2}, \quad (27)$$
$$C = B(1+1/\Omega^2).$$

Again we look at the nonlinear and dispersive coefficients which dictate the evolution of the solitary wave structures. Figure 11 shows how these vary with positron content ranging from 60% to 100%. We see that the nonlinear and dispersive terms are strongly influenced by the proportion of positrons present in the plasma. The nonlinear coefficient A tends to infinity as $\delta \to 1$, whilst the dispersive terms tend to zero. Of course as δ approaches unity, this physically represents a pure electron-positron plasma, so no ions are present, and therefore of course no ion acoustic solitary structures can exist.

For the high positron content plasmas, we also investigate the dependence of the solitary wave excitation on δ—see Figure 12. We note that as for low values of δ, the trend continues that solitons get progressively narrower with smaller
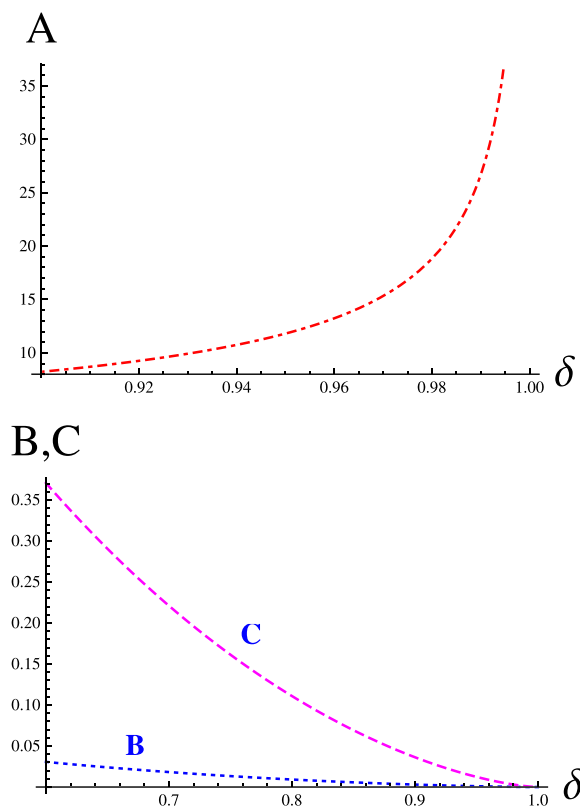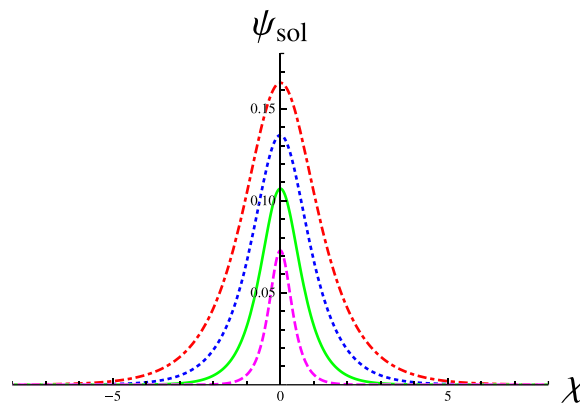

FIG. 12. ψ vs χ for $\delta=0.6$ (red dotted-dashed line), 0.7 (blue dotted line), 0.8 (green continuous line), and 0.9 (purple dashed line), for the particular orientation where $n=0.5$, and $l=m=\sqrt{\frac{1-l^2}{2}}$, taking $\Omega=0.3$, $U=0.1$, $\kappa=3$, and $\theta=1.1$. Based on Eq. (15).

potential, as δ increases. We now look at how soliton shape changes with κ, which represents the degree of superthermality of the plasma. As noted in Figure 8 for low positron content, we also see in Figure 13 that solitons with a low κ value are narrower with smaller amplitude, so increasing superthermality leads to lower amplitude and narrower solitons. We consider in Figure 14 how disparity in temperature between electrons and positrons affects the solitary excitation in plasmas with a high positron content, and note very little variation. This is interesting, as one might expect a greater dependence on proportional temperature differences when the positron-electron ratio is high; however, in reality, according to our model, and looking at Eq. (15), the temperature differential plays only a minor role in the development of solitary wave characteristics. Also we only allow for temperature ratios of up to 1.4, as we feel anything beyond this may be unrealistic. Finally, we analyse the effect of a change of positron concentration and superthermality on the instability of the soliton solution in plasmas with a high positron content. In Figure 15, we see in the upper plot that increases in positron concentration cause the instability growth to be suppressed, as was also observed in the low positron concentration regime earlier. In the lower plot, an
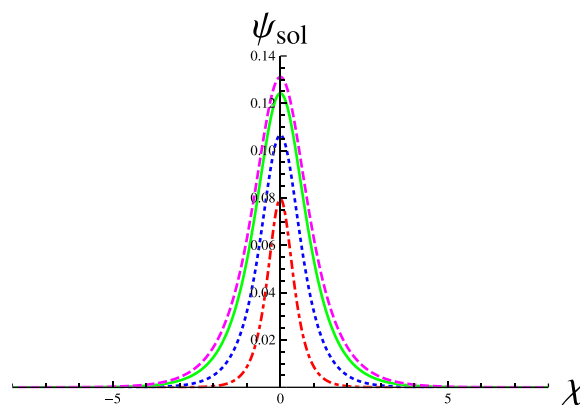

FIG. 11. Upper plot A vs δ, lower plot B, C vs δ for values of δ from 0.6 to 1, setting $\kappa=3$, $\Omega=0.3$, and $\theta=1.1$. Based on Eq. (14).

FIG. 13. ψ vs χ for $\kappa=2$ (red dotted-dashed line), 3 (blue dotted line), 6 (green continuous line), and 12 (purple dashed line), for the particular orientation where $n=0.5$, and $l=m=\sqrt{\frac{1-l^2}{2}}$, taking $\Omega=0.3$, $U=0.1$, $\delta=0.8$, and $\theta=1.1$. Based on Eq. (15).
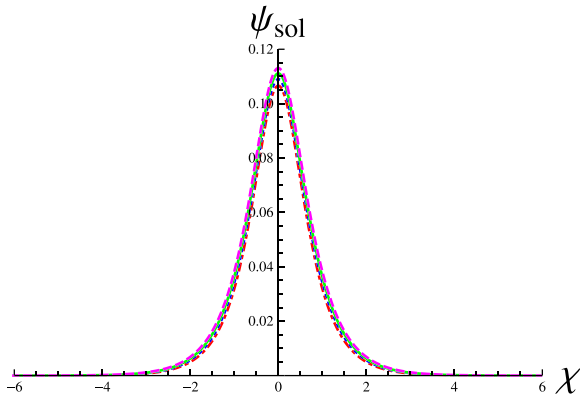
FIG. 14. ψ vs χ for $\theta = 1.1$ (red dotted-dashed line), 1.2 (blue dotted line), 1.3 (green continuous line), and 1.4 (purple dashed line), for the particular orientation where $n = 0.5$, and $l = m = \sqrt{\frac{1-l^2}{2}}$, taking $\Omega = 0.3$, $U = 0.1$, $\delta = 0.8$, and $\kappa = 3$. Based on Eq. (15).

increase in superthermality also causes a decrease in the growth rate of the instability. We can see that in the high positron regime, the instability growth rate is an order of magnitude smaller than in the low positron concentration regime.

VIII. FURTHER SOLUTIONS OF THE ZK EQUATION

A further set of solutions of Eq. (13) was introduced in Ref. 41 using the improved Modified Extended Tanh-Function (iMETF) method.[57] In that method, a solution is anticipated as follows:

$$\psi_1(\zeta) = a_0 + a_1 y + a_2 y^2 + \frac{b_1}{\alpha_1 + y} + \frac{b_2}{(\alpha_2 + y)^2}, \qquad (28)$$

where a_0, a_1, a_2, b_1, b_2 and k are arbitrary constants and y, α_1 and α_2 are functions of ζ to be determined. As in Sec. V, $\zeta = lX + mY + nZ - Ut$, l, m and n are positive real numbers such that $l^2 + m^2 + n^2 = 1$ and U is the incremental soliton velocity. Following Ref. 41, we postulate that

$$\frac{dy}{d\zeta} = k + y^2, \qquad (29)$$

and the general solutions of this equation may be summarized as follows:

For $k < 0$, $y = -\sqrt{-k}\tanh(\sqrt{-k}\zeta)$, or $y = -\sqrt{-k}\coth(\sqrt{-k}\zeta)$. For $k = 0$, $y = -1/\zeta$. For $k > 0$, $y = \sqrt{k}\tan(\sqrt{k}\zeta)$, or $y = \sqrt{k}\cot(\sqrt{k}\zeta)$.

Equations (28) and (29) are substituted into Eq. (13) to achieve a polynomial equation in $y(\zeta)$. The coefficients of y
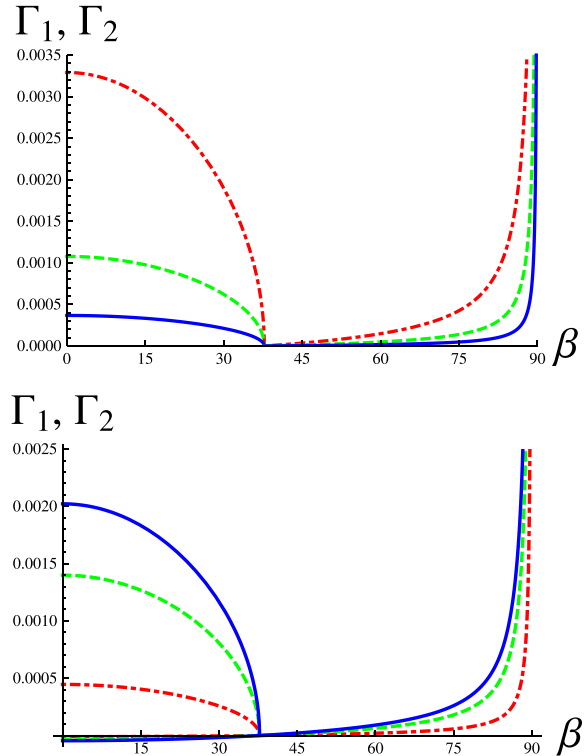

FIG. 15. The first and second order instability growth rate Γ_1 and Γ_2 vs the azimuthal angle β. Upper plot shows $\delta = 0.8$ (red dotted-dashed line), 0.9 (green dashed line), and 0.95 (blue continuous line), taking $\Omega = 0.3$, $\theta = 1.1$, $\kappa = 3$, and wavenumber $k = 0.05$. Lower plot shows $\kappa = 2$ (red dotted-dashed line), 4 (green dashed line), and 12 (blue continuous line), taking $\Omega = 0.3$, $\theta = 1.1$, $\delta = 0.9$, and wavenumber $k = 0.05$. Based on Eqs. (24) and (25).

are equated to zero and the resulting overdetermined system of algebraic differential equations then solved. We find the following solutions for values of $k < 0$:

$$\psi_1 = \frac{U - 8kB_0}{A_0} + \frac{12kB_0}{A_0}\tanh^2(\sqrt{-k}\zeta), \qquad (30)$$

or

$$\psi_1 = \frac{U - 8kB_0}{A_0} + \frac{12kB_0}{A_0}(\tanh^2(\sqrt{-k}\zeta) + \coth^2(\sqrt{-k}\zeta), \qquad (31)$$

where $A_0 = An$, $B_0 = Bn^3 + Cn(l^2 + m^2)$, and A, B, C are as defined in Eq. (14). The solution (30) describes a solitary pulse as shown in Figures 16 and 17 below. It can be seen that the effect of increasing superthermality (lower value of
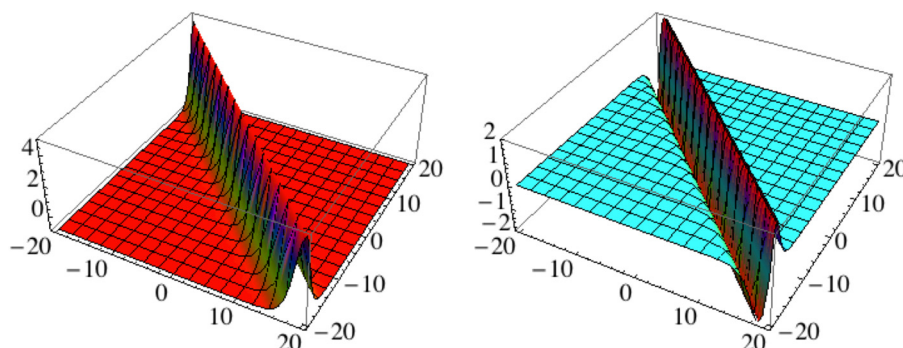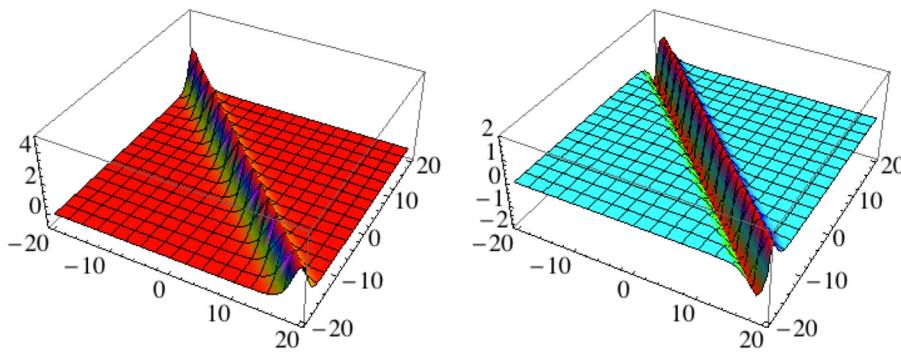

FIG. 16. The profile of a pulse, given by Eq. (30) (left plot), and its corresponding electric field (right plot), in the X-Z plane at time $\tau = 0$ with $m = 0$, $l = n = 1/\sqrt{2}$, $U = 1$, $k = -0.5$ and taking $\Omega = 0.3$, $\theta = 1$, $\delta = 0.2$, and $\kappa = 10$.

FIG. 17. The profile of a pulse, given by Eq. (30) (left plot), and its corresponding electric field (right plot), in the X-Z plane at time $\tau = 0$ with $m = 0$, $l = n = 1/\sqrt{2}$, $U = 1$, $k = -0.5$ and taking $\Omega = 0.3$, $\theta = 1$, $\delta = 0.2$, and $\kappa = 3$.
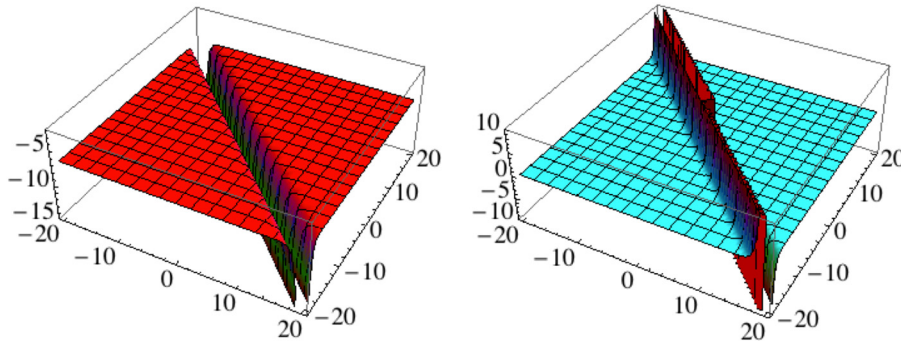

FIG. 18. The profile of an explosive pulse, given by Eq. (31) (left plot), and its corresponding electric field (right plot), in the X-Z plane at time $\tau = 0$ with $m = 0$, $l = n = 1/\sqrt{2}$, $U = 1$, $k = -0.5$ and taking $\Omega = 0.3$, $\theta = 1$, $\delta = 0.2$, and $\kappa = 10$.
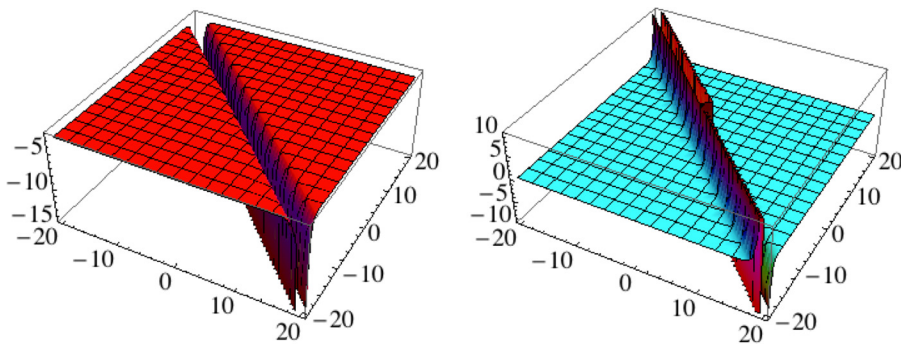

FIG. 19. The profile of a pulse, given by Eq. (31) (left plot), and its corresponding electric field (right plot), in the X-Z plane at time $\tau = 0$ with $m = 0$, $l = n = 1/\sqrt{2}$, $U = 1$, $k = -0.5$ and taking $\Omega = 0.3$, $\theta = 1$, $\delta = 0.2$, and $\kappa = 3$.

FIG. 20. The profile of a train of well-separated explosive periodic pulses, given by Eq. (32) (left plot), and the associated electric field (right plot), in the X-Z plane at time $\tau = 0$ with $m = 0$, u$l = n = 1/\sqrt{2}$, $k = 2$, and taking $\Omega = 0.3$, $\theta = 1$, $\delta = 0.2$, and $\kappa = 10$.
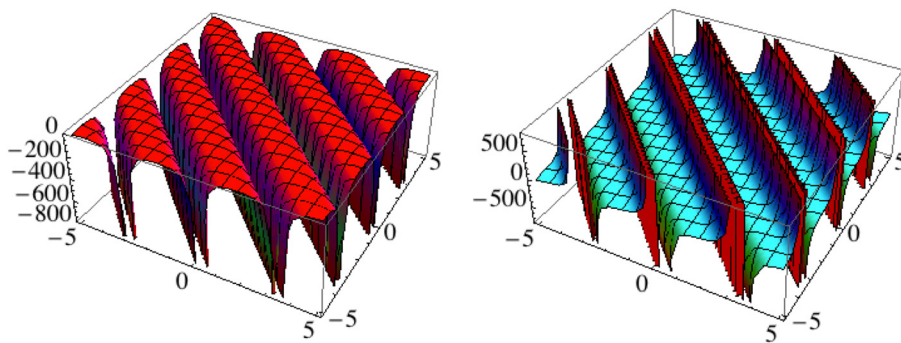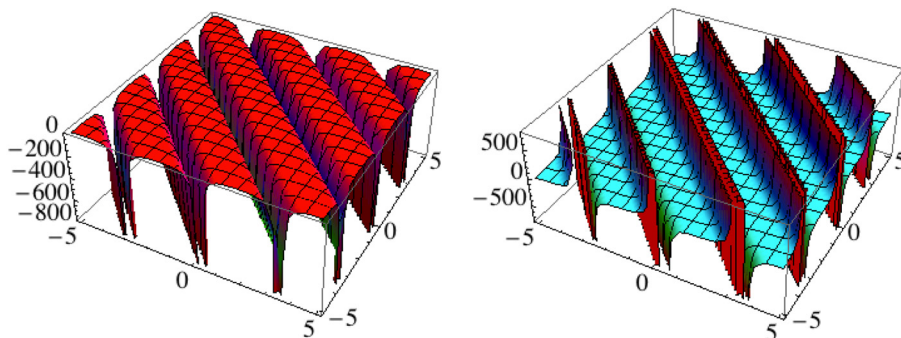

FIG. 21. The profile of a train of well-separated explosive periodic pulses, given by Eq. (32) (left plot), and the associated electric field (right plot), in the X-Z plane at time $\tau = 0$ with $m = 0$, u$l = n = 1/\sqrt{2}$, $k = 2$, and taking $\Omega = 0.3$, $\theta = 1$, $\delta = 0.2$, and $\kappa = 3$.

κ) results in smaller, narrower pulses and more localized electric fields. Note that for $k = -U/4B_0$, the solution recovers the solitary wave solution of Eq. (15). The solution (31) produces an inverted explosive pulse as shown in Figures 18 and 19. It can be seen that the effect of increasing superthermality (lower value of κ) results in smaller, narrower pulses and more localized electric fields.

The following inverted periodic solution (shown in Figures 20 and 21) is obtained using the same method, with $k > 0$:

$$\psi_1 = \frac{U - 8kB_0}{A_0} - \frac{12kB_0}{A_0}\tan^2(\sqrt{k}\zeta). \quad (32)$$

IX. CONCLUSION

Using a fluid model for ion acoustic waves in a magnetized plasma in the presence of background kappa-distributed electrons and positrons, we have derived a linear dispersion relation, and noted a steady decrease in frequency and phase speed due to higher presence of positrons. The frequency in both upper and lower modes is largely unaffected by temperature differences of up to 40% between electrons and positrons.

Through reductive perturbation analysis, we have derived a Zakharov-Kuznetsov equation, modelling ion acoustic solitary waves influenced by the magnetized plasma's nonlinearity and dispersion. Solving this equation using the hyperbolic tangent method, we have found exact analytical expressions for solitary waves. On investigation of the stability of this solution, we have seen that to first order, there is instability up to a critical angle of motion, β_{cr}, and to second order, the solution is unstable for all motion.

A parametric analysis of this solution gives insight into the dependence of the soliton solution on positron concentration. As the positron concentration increases, the solitary wave structures become smaller and narrower. In plasmas with both high and low concentrations of positrons, in conditions of higher superthermality, the dispersive terms of the ZK equation are suppressed, solitary waves have smaller potential amplitudes and narrower widths. The soliton amplitude and width are largely unaffected by a small temperature differential between the electrons and positrons.

Other solutions of the ZK equation have also been investigated, producing solitary and explosive pulse solutions, and periodic solutions.

ACKNOWLEDGMENTS

APPENDIX A: TRANSFORM OF ZK EQ. (13) TO EQ. (18)

Equation (13) is given by

$$\frac{\partial \phi_1}{\partial T} + A\phi_1\frac{\partial \phi_1}{\partial Z} + B\frac{\partial^3 \phi_1}{\partial Z^3} + C\frac{\partial}{\partial Z}\left(\frac{\partial^2 \phi_1}{\partial X^2} + \frac{\partial^2 \phi_1}{\partial Y^2}\right) = 0.$$

We make the following transformations:

$$\phi_1 \to \phi_0\phi', \quad T \to T_0t', \quad X,Y \to L_\perp x', L_\perp y', \quad Z \to L_\| z'.$$

Substituting these values into Eq. (13), and adapting the notation so that subscripts denote partial differentiation gives

$$\frac{\phi_0}{T_0}\partial_{t'}\phi' + A\frac{\phi_0^2}{L_\|}\phi'\partial_{z'}\phi' + B\frac{\phi_0}{L_\|^3}\partial_{z'z'z'}\phi'$$

$$+ C\frac{\phi_0}{L_\| L_\perp^2}\left(\partial_{z'}\partial_{x'x'} + \partial_{z'}\partial_{y'y'}\right)\phi' = 0.$$

We multiply across by T_0/ϕ_0, and cancel primes for simplicity to get

$$\partial_t\phi + \frac{A\phi_0 T_0}{L_\|}\phi\partial_z\phi + \frac{BT_0}{L_\|^3}\partial_{zzz}\phi$$

$$+ \frac{CT_0}{L_\| L_\perp^2}\left(\partial_z\partial_{xx} + \partial_z\partial_{yy}\right)\phi = 0.$$

Now we set $\frac{A\phi_0 T_0}{L_\|} = \frac{BT_0}{L_\|^3} = \frac{CT_0}{L_\| L_\perp^2} = 1$, and this requires that $L_\perp = L_\|(C/B)^{1/2}$, $T_0 = \frac{L_\|^3}{B}$, $\phi_0 = \frac{B}{L_\|^2 A}$. (Note that if we chose to take $L_\| = 1$, we would find $T_0 = \frac{1}{B}$, $\phi_0 = \frac{B}{A}$, and $L_\perp = \left(\frac{C}{B}\right)^{1/2}$.) This results in the following expression:

$$\partial_t\phi + \phi\partial_z\phi + \partial_z(\partial_{xx} + \partial_{yy} + \partial_{zz})\phi = 0.$$

We observe that the magnetic field dependence has been "hidden" in the perpendicular length scale (recalling that $L_\perp \sim \left(\frac{C}{B}\right)^{1/2} = \left(1 + 1/\Omega^2\right)^{1/2}$). Then, by setting $z \to x$, and permutating y and x accordingly we recover Eq. (18). If we also formally set $\phi \to n$, we retrieve Eq. (1.1) from Ref. 55

$$\partial_t n + n\partial_x n + \nabla^2\partial_x n = 0. \quad (A1)$$

APPENDIX B: FROM THE CANONICAL FORM (BY ALLEN AND ROWLANDS[55]) BACK

From Appendix A, the following scaling to convert to the Allen and Rowlands[55] variables has been used:

$Z \to L_\| x$,   where $L_\| \in \Re$ is arbitrary;

$X, Y \to L_\perp y, L_\perp z$,   where $L_\perp = L_\|\left(\frac{C}{B}\right)^{1/2}$;

$\phi \to \phi_0\bar{\phi}$,   where $\phi_0 = \frac{B}{L_\|^2 A}$;

$T \to T_0 t$,   where $T_0 = \frac{L_\|^3}{B}$.

Working in reverse, using Eq. (1.1) of Ref. 55 as our starting point (with $\bar{\phi} = n$ therein), we recover precisely our Eq. (13) upon setting: $x \to \frac{Z}{L_\|}, y, z \to \frac{X}{L_\perp}, \frac{Y}{L_\perp}; \bar{\phi} \to \frac{\phi}{\phi_0}; t \to \frac{T}{T_0}$.

We also note that the k, γ_1 and γ_2 variables in Eqs. (22) and (23) revert, respectively, to $k \to kL_\perp = kL_\|\left(\frac{C}{B}\right)^{1/2}$, $\gamma_1 \to \gamma_1 T_0 = \gamma_1\frac{L_\|^3}{B}$, $\gamma_2 \to \gamma_2 T_0 = \gamma_2\frac{L_\|^3}{B}$.

[1]V. Vasyliunas, J. Geophys. Res. **73**, 2839, doi:10.1029/JA073i009p02839 (1968).

[2]T. P. Armstrong, M. T. Paonessa, E. V. Bell II, and S. M. Krimigis, J. Geophys. Res. **88**, 8893, doi:10.1029/JA088iA11p08893 (1983).

[3]W. G. Pilipp, H. Miggenrieder, M. D. Montgomery, K.-H. Muhlhauser, H. Rosenbauer, and R. Schwenn, J. Geophys. Res. **92**, 1075, doi:10.1029/JA092iA02p01075 (1987).

[4]L. A. Fisk and G. Gloeckler, Astrophys. J. Lett. **640**, L79 (2006).

[5]S. P. Christon, D. G. Mitchell, D. J. Williams, L. A. Frank, C. Y. Huang, and T. E. Eastman, J. Geophys. Res. **93**, 2562, doi:10.1029/JA093iA04p02562 (1988).

[6]V. Pierrard and M. Lazar, Sol. Phys. **267**, 153 (2010).

[7]M. Maksimovic, V. Pierrard, and P. Riley, Geophys. Res. Lett. **24**, 1151, doi:10.1029/97GL00992 (1997).

[8]V. Formisano, G. Moreno, F. Palmiotto, and P. C. Hedgecock, J. Geophys. Res. **78**, 3714, doi:10.1029/JA078i019p03714 (1973).

[9]P. Schippers, M. Blanc, N. André, I. Dandouras, G. R. Lewis, L. K. Gilbert, A. M. Persoon, N. Krupp, D. A. Gurnett, A. J. Coates, S. M. Krimigis, D. T. Young, and M. K. Dougherty, J. Geophys. Res. **113**, 07208, doi:10.1029/2008JA013098 (2008).

[10]M. Hellberg, R. L. Mace, T. K. Baluku, I. Kourakis, and N. S. Saini, Phys. Plasmas **16**, 094701 (2009).

[11]S. Sultana and I. Kourakis, Plasma Phys. Controlled Fusion **53**, 045003 (2011).

[12]S. Sultana, G. Sarri, and I. Kourakis, Phys. Plasmas **19**, 012310 (2012).

[13]T. Baluku and M. Hellberg, Plasma Phys. Controlled Fusion **53**, 095007 (2011).

[14]L. Hau and W. Fu, Phys. Plasmas **14**, 110702 (2007).

[15]N. El-Bedwehy and W. Moslem, Astrophys. Space Sci. **335**, 435 (2011).

[16]M. J. Rees, G. W. Gibbons, S. W. Hawking, and S. Siklaseds, *The Early Universe* (Cambridge University Press, Cambridge, 1983).

[17]J. Daniel and T. Tajima, Astrophys. J. **498**, 296 (1998).

[18]F. C. Michel, Rev. Mod. Phys. **54**, 1 (1982).

[19]P. Goldreich and W. H. Julian, Astrophys. J. **157**, 869 (1969).

[20]J. A. Orosz, R. A. Remillard, C. D. Bailyn, and J. E. McClintock, Astrophys. J. Lett. **478**, L83 (1997).

[21]N. L. Tsintsadze, A. Rasheed, H. A. Shah, and G. Murtaza, Phys. Plasmas **16**, 112307 (2009).

[22]Q. Haque, N. L. Tsintsadze, and W. Masood, Phys. Plasmas **18**, 122106 (2011).

[23]I. V. Moskalenko and A. W. Strong, Astrophys. J. **493**, 694 (1998).

[24]O. Adriani, G. C. Barbarino, G. A. Bazilevskaya, R. Bellotti, M. Boezio, E. A. Bogomolov, L. Bonechi, M. Bongi, V. Bonvicini, S. Bottai, A. Bruno, F. Cafagna, D. Campana, P. Carlson, M. Casolino, G. Castellini, M. P. De Pascale, G. De Rosa, N. De Simone, V. Di Felice, A. M. Galper, L. Grishantseva, P. Hofverberg, S. V. Koldashov, S. Y. Krutkov, A. N. Kvashnin, A. Leonov, V. Malvezzi, L. Marcelli, W. Menn, V. V. Mikhailov, E. Mocchiutti, S. Orsi, G. Osteria, P. Papini, M. Pearce, P. Picozza, M. Ricci, S. B. Ricciarini, M. Simon, R. Sparvoli, P. Spillantini, Y. I. Stozhkov, A. Vacchi, E. Vannuccini, G. Vasilyev, S. A. Voronov, Y. T. Yurkin, G. Zampa, N. Zampa, and V. G. Zverev, Nature **458**, 607 (2009).

[25]E. P. Liang, S. C. Wilks, and M. Tabak, Phys. Rev. Lett. **81**, 4887 (1998).

[26]M. Tinkle, R. G. Greaves, C. M. Surko, R. L. Spencer, and G. W. Mason, Phys. Rev. Lett. **72**, 352 (1994).

[27]R. G. Greaves and C. M. Surko, Phys. Rev. Lett. **75**, 3846 (1995).

[28]G. Gahn, G. D. Tsakiris, G. Pretzler, K. J. Witte, C. Delfin, C. G. Wahlstrom, and D. Habs, Appl. Phys. Lett. **77**, 2662 (2000).

[29]Y. B. Zel'dovich and I. D. Novikov, *Relativistic Astrophysics* (University of Chicago Press, Chicago, IL, 1981).

[30]S. L. Shapiro and S. A. Teakolsky, *Black Holes, White Dwarfs and Neutron Stars: The Physics of Compact Objects* (Wiley-Interscience, New York, 1983).

[31]H. Chen, S. C. Wilks, J. D. Bonlie, E. P. Liang, J. Myatt, D. F. Price, D. D. Meyerhofer, and P. Beiersdorfer, Phys. Rev. Lett. **102**, 105001 (2009).

[32]B. Shen and J. Meyer-ter-Vehn, J. Phys. Rev. E **65**, 016405 (2001).

[33]S. C. Wilks, J. M. Dawson, and W. B. Mori, Phys. Rev. Lett. **69**, 1383 (1992).

[34]J. W. Shearer, J. Garrison, J. Wong, and J. E. Swain, Phys. Rev. A **8**, 1582 (1973).

[35]N. L. Tsintsadze, R. Chaudhary, and A. Rasheed, J. Plasma Phys. **79**, 587 (2013).

[36]G. Sarri, W. Schumaker, A. Di Piazza, M. Vargas, B. Dromey, M. E. Dieckmann, V. Chvykov, A. Maksimchuk, V. Yanovsky, Z. H. He, B. X. Hou, J. A. Nees, A. G. R. Thomas, C. H. Keitel, M. Zepf, and K. Krushelnick, Phys. Rev. Lett. **110**, 255002 (2013).

[37]H. Chen, M. Nakai, Y. Sentoku, Y. Arikawa, H. Azechi, S. Fujioka, C. Keane, S. Kojima, W. Goldstein, B. R. Maddox, N. Miyanaga, T. Morita, T. Nagai, H. Nishimura, T. Ozaki, J. Park, Y. Sakawa, H. Takabe, G. Williams, and Z. Zhang, New J. Phys. **15**, 065010 (2013).

[38]G. Sarri, private communication (2013).

[39]E. Infeld and G. Rowlands, *Nonlinear Waves, Solitons and Chaos* (Cambridge University Press, Cambridge, 2000).

[40]V. Zakharov and E. Kuznetzov, Sov. Phys. JETP **39**, 285 (1974).

[41]I. Kourakis, W. M. Moslem, U. M. Abdelsalam, R. Sabry, and P. K. Shukla, Plasma Fusion Res. **4**, 18 (2009).

[42]Q. Qu, B. Tian, W. Liu, K. Sun, P. Wang, Y. Jiang, and B. Qin, Eur. Phys. J. D **61**, 709 (2011).

[43]E. F. El-Shamy and N. A. El-Bedwehy, Phys. Lett. A **374**, 4425 (2010).

[44]G. Williams and I. Kourakis, Plasma Phys. Controlled Fusion **55**, 055005 (2013).

[45]Y. H. Ichikawa, T. Imamura, and T. Taniuti, J. Phys. Soc. Jpn **33**, 189 (1972).

[46]P. Frycz and E. Infeld, J. Plasma Phys. **41**, 441 (1989).

[47]N. S. Saini, I. Kourakis, and M. A. Hellberg, Phys. Plasmas **16**, 062903 (2009).

[48]D. Swanson, *Plasma Waves*, 2nd ed. (IOP Publishing Ltd., New York, 2003), pp. 107–109.

[49]E. Infeld, J. Plasma Phys. **33**, 171 (1985).

[50]B. Shivamoggi, J. Plasma Phys. **41**, 83 (1989).

[51]W. Malfliet and W. Hereman, Phys. Scr. **54**, 563 (1996).

[52]W. Moslem and R. Sabry, Chaos, Solitons Fractals **36**, 628 (2008).

[53]S. Sultana and I. Kourakis, Eur. Phys. J. D **66**, 100 (2012).

[54]M. A. Allen and G. Rowlands, J. Plasma Phys. **50**, 413 (1993).

[55]M. A. Allen and G. Rowlands, J. Plasma Phys. **53**, 63 (1995).

[56]K. P. Das and F. Verheest, J. Plasma Phys. **41**, 139 (1989).

[57]R. Sabry, W. M. Moslem, and P. K. Shukla, Phys. Lett. A **372**, 5691 (2008).